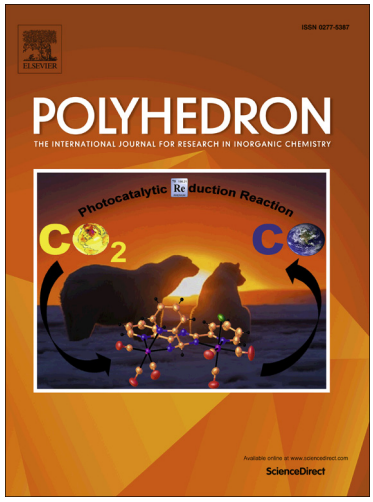

Synthesis, characterization, cytotoxicity and antimicrobial studies on Bi(III) dithiocarbamate complexes containing furfuryl group and their use for the preparation of Bi_2O_3 nanoparticles

Sundaramoorthy Tamilvanan, Govindasamy Gurumoorthy, Subbiah Thirumaran, samuele Ciattini

PII: S0277-5387(16)30468-5
DOI: http://dx.doi.org/10.1016/j.poly.2016.09.038
Reference: POLY 12226

To appear in: *Polyhedron*

Received Date: 18 May 2016
Revised Date: 15 September 2016
Accepted Date: 21 September 2016

Please cite this article as: S. Tamilvanan, G. Gurumoorthy, S. Thirumaran, s. Ciattini, Synthesis, characterization, cytotoxicity and antimicrobial studies on Bi(III) dithiocarbamate complexes containing furfuryl group and their use for the preparation of Bi_2O_3 nanoparticles, *Polyhedron* (2016), doi: http://dx.doi.org/10.1016/j.poly.2016.09.038

Synthesis, characterization, cytotoxicity and antimicrobial studies on Bi(III) dithiocarbamate complexes containing furfuryl group and their use for the preparation of Bi_2O_3 nanoparticles

Sundaramoorthy Tamilvanan[a], Govindasamy Gurumoorthy[b], Subbiah Thirumaran[b]* and samuele Ciattini[c]

[a]Chemistry section [FEAT], Annamalai University, Annamalainagar, Tamilnadu 608002, India
[b]Department of Chemistry, Annamalai University, Annamalainagar, Tamilnadu 608002, India
[c]Centro di Cristallografia strutturale, Polo Scientifio di Sesto Fiorentino, Via della Lastruccia No.3, 50019 Sesto Fiorentino, Firenze, Italy

*Corresponding author
Dr. S. Thirumaran
Department of Chemistry
Annamalai University
Annamalainagar 608 002
Tamil Nadu, INDIA
Tel: +91 9842897597
E-mail: sthirumaran@yahoo.com

Synthesis, characterization, cytotoxicity and antimicrobial studies on Bi(III) dithiocarbamate complexes containing furfuryl group and their use for the preparation of Bi_2O_3 nanoparticles

Sundaramoorthy Tamilvanan[a], Govindasamy Gurumoorthy[b], Subbiah Thirumaran[b]* and samuele Ciattini [c]

[a]Chemistry section [FEAT], Annamalai University, Annamalainagar, Tamilnadu 608002, India
[b]Department of Chemistry, Annamalai University, Annamalainagar, Tamilnadu 608002, India
[c]Centro di Cristallografia strutturale, Polo Scientifio di Sesto Fiorentino, Via della Lastruccia No.3, 50019 Sesto Fiorentino, Firenze, Italy.

Correspondence e-mail: sthirumaran@yahoo.com

Abstract

Bismuth(III) dithiocarbamate complexes, tris(N-furfuryl-N-propyldithiocarbamato-S,S')bismuth(III) (**1**), tris(N-furfuryl-N-butyldithiocarbamato-S,S')bismuth(III) (**2**) and tris(N-furfuryl-N-benzyldithiocarbamato-S,S')bismuth(III) (**3**), have been prepared and characterized by microanalysis, and spectroscopy (IR and NMR). Structure of **3** has been obtained by single crystal X-ray diffraction. This complex contains distorted pentagonal pyramidal Bi(III) centres which attain an overall distorted pentagonal bipyramidal coordination via long range intermolecular Bi···S interactions. DFT quantum mechanical studies of **3** were carried out, supporting the partial double bond character of C–N (thioureide) and C–S bonds in dithiocarbamate ligands. All the compounds have been screened against a panel of microbes *viz. Vibrio cholerae, Bacillus subtilis*, *Klebsiella pneumoniae*, *Escherichia coli, Staphylococcus aureus, Aspergillus niger* and *Candida albicans.* Complexes **1** and **3** were found to have better activity against *K. pneumoniae, V. cholerae*, *A. niger* and *C. albicans* than the complex **2**. Complexes **1-3** have been evaluated for their *in vitro* cytotoxic activity against KB cells. Complexes **1** and **3** showed higher activity than **2**. Bi_2O_3 obtained from thermal decomposition of **3** has been characterized by PXRD, HRTEM, EDAX, UV-Vis and Fluorescence spectroscopy. PXRD study showed that the sample is composed of monoclinic phase of α-Bi_2O_3. Photocatalytic activity of as-prepared α-Bi_2O_3 was determined by decolourization of rhodamine-B in aqueous solution under ultra violet irradiation.

Keywords : Bismuth(III) dithiocarbamates; antimicrobial; cytotoxicity; bismuth oxide nanoparticles; photodegradation.

1. Introduction

A growing interest in dithiocarbamate chemistry is due to their structural diversity and a wide range of applications in industries as rubber vulcanization accelerators, flotation agents in metallurgy, heavy metal scavengers from waste and as effective antidotes for cadmium detoxication [1-4]. The chemistry of bismuth dithiocarbamates of the general formula $Bi(S_2CNR_2)_3$ is a subject of increasing interest during the last decades considering their utility for the preparation of bismuth sulfide nanoparticles [5-6]. The coordination chemistry of Bi(III) with dithiocarbamates is dominated by intermolecular interactions which lead to polymeric structures [7]. The supramolecular aggregation is determined by steric bulk of ligand bound R substituents. The presence of bulky R substituents often precludes supramolecular aggregation via secondary M···S interactions whereas smaller R groups allow for the formation of such interactions [8]. A review by Buac *et al* [9]. shows dithiocarbamate complexes with various metals as a new type of potent proteasomes inhibitors in human cancer cells. Proteasome inhibition has emerged recently as a novel approach to cancer therapy with first-in-class proteasome inhibitor bortezomib. Bortezomib is used for treatment of multiple Myeloma in the clinic from 2003 [10]. Nagy *et al.* review promising results of recent research in anticancer activity of dithiocarbamate complexes with noble metals (such as platinum, palladium, copper, ruthenium and gold) and their mechanism of action [11]. Metal dithiocarbamate (M=Pt(IV) , Pd(II) ,Sn(IV) ,Ru(I), Au(III)) complexes have also been investigated for their anti-cancer potential [12]. Recently the Bismuth dithiocarbamate complexes were shown to be potent *in vitro* cytotoxicity against various human cancer cell lines [13,14]. Synthesis and study of physical properties of semiconducting nanoparticles have been the subject of active research during the past decade [15,16]. Bismuth oxide nanoparticles have been used as a material for optical coatings, photovoltaics and microwave integrated circuits superconductor [17-19]. The aim of this work is to prepare

new Bi(III) dithiocarbamate complexes, and to study their application. In this paper, we report synthesis, spectral, antimicrobial and cytotoxicity studies on three Bi(III) dithiocarbamate complexes **1-3.** Crystal structure of **3** is reported. In addition, preparation of bismuth oxide nanobars from complex **3** and its photocatalytic activity is also presented.

2. Experimental

2.1. Materials and physical measurements

All materials and solvents were analytical grade and used without further purification. Melting points were determined by thermal melting point apparatus and used with open capillary tubes and are uncorrected. Elemental analysis for carbon, hydrogen and nitrogen were carried out with varioMICRO V2.2.0 elemental analyser. The IR spectra were recorded on a SHIMADZU FT-IR spectrophotometer in the frequency range 4000–400 cm^{-1} as KBr pellets of the complexes. ^{1}H and ^{13}C NMR spectra were recorded with a Bruker 400 MHz NMR instruments at room temperature using $CDCl_3$ as a solvent and TMS as an internal reference. TECNAI T2 G2 make-FEI instrument was used to record HRTEM images and Powder X-Ray diffraction patterns were recorded using XPERT-PRO. Fluorescence and UV-vis absorption spectra were recorded on Perkin Elmer L555 and SHIMADZU UV-1650 PC, respectively. EDAX are performed by SUPRA 55VP CARL.

2.2. X-ray crystallography

Suitable single crystals were obtained by the slow evaporation of complex **3** from acetone at room temperature. The crystal diffraction data of complex **3** were collected on an Xcalibur, Sapphire3 diffractometer equipped with a graphite monochromated MoK_{α} radiation (λ = 0.71073) at ambient temperature. The structure was solved and refined by direct method using SHELXL-2014/7 (Sheldrick, 2014) [20]. All the non-hydrogen atoms

were refined anisotropically and the hydrogen atoms were refined isotropically. Details of the crystal data and structure refinement parameters for **3** are summarized in **Table 1**.

2.3 Computational methods

DFT studies were performed with GAUSSIAN-09 program package with the aid of the Gauss View visualization program [21]. Molecular geometry was optimized with DFT using basic set of LANL2DZ and calculation method of B3LYP.

2.4. Synthesis of complexes

2.4.1. Preparation of amines

N-furfuryl-N-propylamine , N-furfuryl-N-butylamine and N-furfuryl-N-benzylamine were prepared by general methods reported as earlier [22].

2.4.2. Preparation of complex 1

N-furfuryl-N-propylamine (0.88 g, 6.0 mmol,) and carbon disulfide (0.36 mL, 6.0 mmol) were dissolved in ethanol (20 ml) and stirred for 30 min under ice cold condition. $Bi(NO_3)_3.5H_2O$ (0.96g, 2mmol) was dissolved in 50 ml of water and added to the solution. A pale yellow solids were obtained by filtration. The product was recrystallised in acetone (**Scheme 1**). Yield: 78%; m.p. 115-117°C; IR (KBr (ν/cm^{-1}): 1478 (ν_{C-N}); 1012 (ν_{C-S}); ^{1}H NMR ($CDCl_3$); δ = 0.92 (t, 9H, N–CH_2–CH_2–CH_3); 1.76 (m, 6H, N–CH_2–CH_2–CH_3); 3.76(t, 6H, N–CH_2–CH_2–CH_3); 5.07 (s, 6H, CH_2 furfuryl); 6.43 (d, 3H, H–3 (furyl); 6.36 (dd, 3H, H–4 (furyl); 7.38 (d, 3H, H–5 (furyl); ^{13}C NMR ($CDCl_3$); δ = 11.3 (CH_2-CH_2-CH_3); 20.1 (CH_2-CH_2-CH_3); 49.6 (CH_2-CH_2-CH_3); 55.3 (CH_2 furfuryl); 110.3, 142.4, 148.9 (furyl ring carbons); 203.1 (NCS_2). Anal, Calc. for $C_{27}H_{36}BiN_3O_3S_6$(%) : C, 38.06; H, 4.26; N, 4.93. Found: C, 37.94; H, 4.11; N, 4.89.

2.4.3 Preparation of complex 2

A method similar to that described for the synthesis of **1** was adopted; However N-furfuryl-N-butylamine was used instead of N-furfuryl-N-propylamine. Yield: 84%; m.p. 116-118°C; IR (KBr (ν/cm^{-1}): 1478 ($\nu_{C\text{-}N}$); 1011 ($\nu_{(C\text{-}S)}$; ^{1}H NMR ($CDCl_3$); δ = 0.94 (t, 9H, N–CH_2–CH_2–CH_2–CH_3); 1.34 (m, 6H, N–CH_2–CH_2–CH_2–CH_3); 1.71 (m, 6H, N–CH_2–CH_2–CH_2–CH_3); 3.79 (t, 6H, N–CH_2–CH_2–CH_2–CH_3); 5.06 (s, 6H, CH_2 furfuryl); 6.43 (d, 3H, H–3 (furyl); 6.37 (dd, 3H, H–4 (furyl); 7.39 (d, 3H, H–5 (furyl). ^{13}C NMR ($CDCl_3$); δ = 13.7 (CH_2-CH_2-CH_2-CH_3); 20.1 (CH_2-CH_2-CH_2-CH_3), 28.6 (CH_2-CH_2-CH_2-CH_3); 49.5 (CH_2-CH_2-CH_2-CH_3); 53.6 (CH_2 furfuryl); 110.4, 142.5, 148.8 (furyl ring carbons); 202.7 (NCS_2). Anal, Calc. for $C_{30}H_{42}BiN_3O_3S_6$(%): C, 40.30; H, 4.74; N, 4.70. Found: C, 40.12; H, 4.68; N, 4.72.

2.4.4 Preparation of complex 3

A method similar to that described for the synthesis of **1** was adopted; However N-furfuryl-N-benzylamine was used instead of N-furfuryl-N-propylamine. Yield: 67%; m.p.127-129°C; IR (KBr (ν/cm^{-1}): 1465 ($\nu_{C\text{-}N}$); 1012 ($\nu_{C\text{-}S}$); ^{1}H NMR ($CDCl_3$); δ= 5.00(6H, s, N-CH_2-C_6H_5); 5.19 (6H, s, CH_2 furfuryl) ; 6.35-7.39 (aromatic protons); ^{13}C NMR ($CDCl_3$); δ= 48.0 (CH_2-C_6H_5); 55.9 (CH_2 furfuryl), 110.4,110.6,142.6, 148.6 (furyl ring carbons); 128.0, 128.1, 128.8, 134.9 (phenyl ring carbons); 204.7 (NCS_2). Anal, Calc. for $C_{39}H_{36}BiN_3O_3S_6$(%): C, 47.03; H, 3.64; N, 4.22. Found: C, 46.90; H, 3.65; N, 4.18.

2.4.5 Preparation of bismuth oxide nanoparticles

The bismuth oxide nanoparticles were prepared by thermal decomposition of complex **3**. 1.5 g of complex **3** was placed in muffle-furnace at 500°C for 30 min in the presence air atmosphere. The final residue analyzed to α-Bi_2O_3.

3. Biological assays

3.1 Antimicrobial assay

The cultures of microorganism were spreaded on the incubated test plates (Mueller Hinton Agar) [23]. The sterile antibiotic discs (diameter of 6 mm) loaded with required concentrations (400 and 800 μg/ml) of complexes **1, 2** and **3** were placed on the plates. The plates were incubated for 24 h at 37ºC. After that, the zones of inhibition were examined and read the diameter as the activity against the tested microorganism.

3.2 Cytotoxicity assay

The cytotoxic activity of complexes **1**-**3** in KB cells was determined by the MTT assay [24]. The KB Cells (1×10^6 cells/ml) were seeded into a 96 well plate and incubated at 37°C in 5% CO_2 atmosphere for 24 hours. Then the KB cells were treated with different concentrations (0-1000 μg/ml) of complexes **1**, **2** and **3.** After 24 h incubation with complexes , the cells were further incubated at 5% CO_2 at 37°C for 24 h. 0.5 mg/ml MTT dye was added. Then color was allowed to develop for additional 4 h incubation. An equal amount of DMSO was added to stop the reaction and to solublize the formazan crystals. Absorbance was measured colorimetrically at 570 nm. The percentage of cytotoxic activity was calculated as follows:

% Cytotoxicty = Test optical density / Control optical density X 100

4. Photocatalytic experiments

HEBER Multi Lamp Photo Reactor was used for photo catalytic experiment. The photocatalytic performance of the bismuth oxide was evaluated through the photocatalytic degradation of rhodamine-B. Double distilled water was used to prepare all solutions. In a typical photocatalytic experiments, 0.1 g of as-prepared α-Bi_2O_3 was added to 250 ml of aqueous solution of rhodamine-B in the concentration of 0.01 M. The suspensions were magnetically stirred under darkness for 1 h to reach the adsorption–desorption equilibrium.

The suspension was irradiated by UV light from mercury vapour lamp in a photocatalytic instrument with water cooling device. At certain time intervals, 3 ml of suspension was centrifuged to remove the photocatalyst and analysed by UV-visible spectrophotometer at a wavelength of 554 nm. The measurements were carried out upto 180 min [25].

5. Results and discussion

5.1. Infrared spectral studies

Infrared spectra of complexes **1-3** are shown in **Fig. S1**-**S3**. The infrared absorption spectra of the metal dithiocarbamate complexes have proven to be an important tool in the analysis of the coordination mode (monodentate or bidentate) of the dithiocarbamate ligands [26]. In the present study, the $\nu_{C\text{-}S}$ band is observed at 1012 cm^{-1} for all complexes. The values of the $\nu_{C\text{-}S}$ indicate a bidentate chelating mode of the ligand towards the metal cation [27]. In all the spectra, a strong band appeared in the range of 1445-1480 cm^{-1} is assigned to the C–N (thioureide) stretching mode. This band is characteristic of C–N (thioureide) bond which lies between the single and double bond energies, indicating the partial double bond character [27,28].

5.2 ^{1}H and ^{13}C NMR spectral studies

^{1}H and ^{13}C NMR spectra of complexes **1- 3** are given in **Fig. S4-S9**. Proton NMR spectra were characteristic of each ligand type. Thus N-furfuryl-N-propyldithiocarbamate complex **1** showed three signals (0.92, 1.76 and 3.76 ppm) associated with the methylene and methyl group of propyl that bound to nitrogen appearing at relatively lowfield, together with a sharp singlet (5.07 ppm) assigned to the methylene of furfuryl moiety. For complex **2**, signals observed at 5.06 and 3.79 ppm are due to methylene protons of furfuryl and NCH_2 (butyl) protons, respectively. The remaining signals in the aliphatic region are assigned to the other methylene protons and methyl protons of butyl groups. Two singlets observed in the

aliphatic region are due to the methylene protons of furfuryl and benzyl groups. In all the complexes, methylene protons adjacent to nitrogen atom are deshielded to a large extent on complexation compared to the free amines.

The $N^{13}CS_2$ carbon signals are appeared in the expected region (around 200 ppm) for main group metal dithiocarbamate complexes [29]. In complexes **1-3,** these signals are observed around 203 ppm, indicating contribution of double-bond character to a formally single N–C bond in the dithiocarbamate. For complexes **1-3**, the signals for methylene carbons adjacent to nitrogen atoms are observed in the region 48.0-55.9 ppm. The other two and three signals appeared in the aliphatic region for complexes **1** and **2**, respectively are assigned to the remaining carbons of propyl and butyl groups.

5.3 Single crystal X-ray diffraction analysis of 3

ORTEP diagram of complex **3** is shown in **Fig. 1**. Selected parameters of bond distances and angles are listed in **Table 2**. Complex **3** was crystallised from acetone to give yellow crystals. The central bismuth is six coordinated. Bi has bonded to six crystallographically independent sulfur atoms with Bi–S distances ranging from 2.5876(12) Å to 2.9055(13) Å (**Table 2**) forming a distorted pentagonal pyramid coordination sphere with the shortest distance (Bi–S4 = 2.5876(12) Å) to the S4 atom at the apex. Five sulfur atoms (S2-S6) in the equatorial plane and the central atom (Bi) are not coplanar. S2 atom shows maximum deviation (–0.415 (1) Å) from the mean plane of the atoms S2-S6 and Bi. Furthermore, due to the constraint of the chelate, the angle S1-Bi-S2 being axial is 65.65(3)°, which deviate from the angle 90°. From this, the Bi atom of this complex is in the distorted pentagonal pyramidal configuration.

The short C–N (thioureide) bond distances [C1–N1 = 1.327(6) Å, C14–N2 = 1.357(6) Å and C27–N3 = 1.324(6) Å] indicates that the π-electron density is delocalized over NCS_2. The C–S bond distances [mean: 1.7188(5) Å] are lower than C–S single bond length of 1.81 Å and longer than C–S double bond distance of 1.69 Å. The observed values indicate partial double bond character.

A long Bi···S and C–H···O contacts of 3.340 Å and 2.967 Å, respectively leads to the dimeric association of molecules in the crystal structure as shown in **Fig. 2.** In the crystal structure, neighbouring molecules linked by C–H···π (chelate) and pairs of C–H···π [C11–H11···Cg1 (O3, C29–C32) = 2.790 Å and C5–H5···Cg2 (O2, C16–C19) = 2.671 Å] contacts, thus generating supramolecular network (**Fig. 3**). A weak intramolecular interaction C–H···π (chelate ring, (Bi, S1, S2, C1)) is also found in this complex (**Fig. S10**). Various intramolecular C–H···O and C–H···S hydrogen bonds are observed (**Figs. S11** and **S12**).

5.4 DFT calculations of complex 3.

Optimized structure of complex **3** is given in **Fig. S13.** Optimized geometrical parameters are compared with experimental geometrical parameters (**Table 3**). Theoretically calculated Bi–S bond lengths are greater than those of the experimental data. This may be due to the free isolated molecule is optimized, so the intermolecular interactions are not included which is obvious in solid. The optimized energy and dipolemoment of the complex are -1963.52 a.u. and 3.92 Debye. The C–N(thioureide) and C–S distances are almost equal in both the cases. This observation also supports the delocalization of π-electron density over S_2CN moiety [30].

5.5 Frontier molecular orbital analysis

Frontier molecular orbital densities can be used to describe the reactivity of a particular atom in the molecule. According to frontier electron reactivity theory, the chemical reaction takes place at a position where overlap of the HOMO and LUMO are the maximum. In the case of donor and acceptor molecule, the HOMO density and LUMO density respectively are important. The HOMO and LUMO energies are directly related to the ionization potential and electron affinity, respectively. The 3D plots of the HOMO and LUMO energy levels and energy gaps for the complex **3** are shown in **Fig. 4.** These reveal that sulfur atoms have the ability to donate electron and Bi, C and N atoms act as electron acceptor. HOMO-LUMO orbital studies imply that the electron density from the N is transferred to S in the complex. The energy gap between the HOMO and LUMO is 3.7496 eV. The large energy gap reveals that the complex is stable. The hardness of the complex is 1.8748 eV [31].

5.6 Molecular Electrostatic Potential

Molecular electrostatic potential is related to the electronic density and is useful to determine the sites for electrophilic and nucleophilic reactions. The MEP surface and electrostatic potential contour maps are shown in **Fig. 5.** The MEP surface shows the negative region(red) of the MEP related to electrophilic reactivity and the positive regions (blue) of the MEP related to nucleophilic reactivity. Electrostatic potential surface energies are in the range from −396.54 (red) to +396.54 (blue) $kJmol^{-1}$ [32]. Calculated electrostatic potential surfaces are generated at an isodensity of 0.02 a.u. MEP surface diagram shows that the complex has possible site for electrophilic attack (red region on S) and a site for nucleophilic attack (blue region on N).

5.7 Antimicrobial studies

The antibacterial study was conducted against *Vibrio cholerae, Bacillus subtilis*, *Klebsiella pneumoniae*, *Escherichia coli* and *Staphylococcus aureus,* using the disc diffusion method. Ciprofloxacin was used as the reference drug. The results of the complexes are shown in **Fig. 6.** The antibacterial study exhibited that all the complexes have no effect towards *B.substils* and *S.aureus.* All the complexes demonstrated lower activity against *E.coli.* Complexes **1** and **3** showed better activity towards *K.pneumoniae* and *V.cholerae* than complex **2.** The antifungal studies revealed that the complexes **1** and **3** have higher activity against all tested fungi than the complex **2.** Generally, the antimicrobial studies indicated that the activity of the complexes follows the order: **1 ~ 3 >2.**

5.8 *In vitro* cytotoxicity

The cytoxic activity of bismuth(III) dithiocarbamates **1-3** was evaluated. Microscopic images of control and apoptic morphological changes in KB (oral) cell line treated with complexes **1-3** are shown in **Fig. S14**. The graph for the cytotoxic effect against KB(oral) cells after 24 h treatment using all three complexes **1-3** are presented in **Fig. 7**. Figure **7** showed that complexes **1** and **2** were able to effectively kill about 70% of the cell population, whereas complex **3** kills 98% of the cell population at the concentration 500 µg/ml. Complexes **1** and **3** display the *in vitro* cytotoxic activity against KB(oral) cells with IC_{50} values of 44 and 40 µg/ml, respectively, while the complex **2** has low activity (IC_{50} = 85 µg/ml). Apparently, the ligands especially N-bound organic moieties play an important role in the antiproliferative action of the complexes.

5.9 Characterization of Bismuth oxide nanoparticles

The powder X-ray diffraction pattern for α-Bi_2O_3 is shown in **Fig. 8**. The peaks in the diffraction pattern is characteristics of the monoclinic phase of α-Bi_2O_3, which are in good agreement with the reported pattern (JCPDS file No: 76-1730) [33, 34]. The observed narrow peak at (1 2 0) for α-Bi_2O_3 reveals that the particles are elongated towards the c-axis which is characteristic of the bar shaped nanoparticles.

HRTEM images (**Fig. 9a** and **9b**) of as-prepared α-Bi_2O_3 display that the obtained products are nanobars. The width and length of the nanobars are in the range 24-40 nm and 75-200 nm. The d spacing calculated from high magnification HRTEM was found to be 2.48 Å corresponding to the (1 2 0) plane for α-Bi_2O_3 and also supports the XRD analysis. SAED pattern of Bi_2O_3 confirms that the obtained products are in crystalline nature. The elemental composition of the as-prepared α-Bi_2O_3 was studied by EDS analysis. The energy dispersive X-ray spectrum is given in **Fig. S15**.

EDS confirms the obtained products are Bi_2O_3. A peak due to sulfur is not observed. This confirms that no bismuth sulfide is formed by thermal decomposition of **3**. The formation of Bi_2O_3 is further supported by the fact that Bi_2O_3 was obtained as a final residue in the thermal decomposition of Bi(III) dithiocarbamate complexes in air atmosphere [35].

UV-Vis absorption and photoluminescence spectra of as-prepared α-Bi_2O_3 are shown in **Fig. 10**. An absorption band appeared at 253 nm (4.90 eV) is attributed to the first exciton absorption of α-Bi_2O_3 nanobars. The blue shift of the absorption band of the as-prepared α-Bi_2O_3 compared to bulk Bi_2O_3 (435 nm, 2.85 eV) displays the quantum confinement effect of α-Bi_2O_3 nanobars [36]. The observed peak at 369 nm in the photoluminescence spectrum of Bi_2O_3 is commonly attributed to the excitonic or band edge emission. The

photoluminescence peak position of band edge emission of nanomaterials is strongly size dependent.

5.10 Dye degradation by UV light irradiated as-prepared Bi_2O_3.

The use of metal oxides and metal sulfides for decomposition of pollutants such as dyes has received considerable recent attention. Particularly, Bi_2O_3 is considered as a good photocatalyst used for degradation of dyes under UV irradiation . The photocatalytic activity of Bi_2O_3 prepared here are therefore of interest. The absorptions of UV light irradiated sample (aqueous solution of rhodamine-B and as-prepared Bi_2O_3) at various time intervals (30, 60, 90, 120, 150 and 180 min) were recorded to study the photocatalytic activities of as-prepared Bi_2O_3. The percentage of dye degradation was defined by the following formula:

$$\% \text{ of degradation} = \frac{A_0 - A_t}{A_0} X\ 100$$

Where A_0 is the initial absorbance of dye; A_t is the absorbance of dye at time t. Aqueous solution of rhodamine-B without catalyst shows small degradation when irradiated with UV light. **Fig. 11** shows time-dependent UV-Vis absorption spectra of rhodamine-B during photoirradiation with as-prepared Bi_2O_3 under ultra violet light. The percentage of decolorization efficiency of Bi_2O_3 is 92 %.

6. Conclusions

Complexes **1-3** have been prepared and characterized. Bismuth atom in the mononuclear complex exists within an S_6 donor set that defines a distorted pentagonal pyramidal geometry. Computational studies on complex **3** were carried out. IR spectral, structural and DFT studies confirm the partial π-conjugation over the NCS_2 group. All the

complexes were screened for *in vitro* antibacterial and antifungal activities. These results exhibited that complexes **1** and **3** showed good antimicrobial activity against selected bacterial strains and fungal strains than **2.** The cytotoxicity of complexes **1-3** against KB cells have been evaluated. Complexes **1** and **3** (IC_{50} = 44 and 40 µg/ml, respectively) revealed higher activity than **2** (IC_{50} = 85 µg/ml). This study show that the modification of N-bound organic moiety in dithiocarbamate ligands may increase the antimicrobial and cytotoxic activities. α-Bi_2O_3 nanoparticles were obtained from the thermal decomposition of **3** and characterized. UV-Vis spectral studies on α-Bi_2O_3 established pronounced quantum confinement effect. The as-prepared α-Bi_2O_3 functions as photocatalyst for the degradation of rhodamine-B.

7. Supplementary data

CCDC 1479695 contains the supplementary crystallographic data for **3**. This data can be obtained free of charge via http://www.ccdc.cam.ac.uk/conts/retrieving.html, or from the Cambridge Crystallographic Data Centre, 12 Union Road, Cambridge CB2 1EZ, UK; fax: (+44) 1223-336-033; or e-mail: deposit@ccdc.cam.ac.uk.

References

[1] P. J. Nieuwenhuizen , A. W. Ehlers , J. G. Haasnoot , S. R. Janse , J. Reedijk , E. J. Baerends, J. Am. Chem. Soc. **121** (1999) 163-168.

[2] M. J. Cox, E. R. T. Tiekink, Rev. Inorg. Chem. **17** (1997) 1-23.

[3] K. W. Weissmahr, C. L. Houghton, D. L. Sedlak, Anal. Chem. **70** (1998) 4800-4804.

[4] Handong Yin , Feng Li, Daqi Wang, J. Coord. Chem. **60** (2007) 1133-1141.

[5] O. C. Monterio, H. I. S. Nogueiva, T.Trindade, Chem. Mater. **13** (2001) 2103-2111.

[6] R. Chauhan, J. Chaturvedi, M. Trivedi, J. Singh, K. C. Molloy, G. K. Köhn, P. Dinesh. Amalnerkar, A. Kumar, Inorg. Chim. Acta. **430** (2015) 168-175.

[7] Y. W. Koh, C. S. Lai, A. Y. Du, E. R. T. Tiekink, K. P Loh, Chem. Mater. **15** (2003) 4544-4554.

[8] E. R. T. Tiekink, CrystEngComm. **5** (2003) 101-113.

[9] D. Buac, S. Schmitt, G. Ventro, F.R. Kona, Q.P. Dou, Mini. Rev. Med. Chem. **12** (2012) 1193-1201.

[10] Z. Skrott, B. Cvek, Mini. Rev. Med. Chem. **12** (2012) 1184-1192.

[11] E. M. Nagy, L. Ronconi, C. Nardon, D. Freqona, Mini. Rev. Med. Chem. **12** (2012) 1216-1229.

[12] H. Li, C. S. Lai, J. Wu, P. C. Ho, D. de Vos, E. R. T. Tiekink, J. Inorg. Biochem. **101** (2007) 809-816.

[13] N. Zhang, Y. Tai, M. Li, P. Ma, J. Zhao, J. Niu, Dalton Trans. **43** (2014) 5182-5189.

[14] I. I. Ozturk, C. N. Banti, N. Kourkoumelis, M. J. Manos, A. J. Tasiopoulos, A. M. Owczarzak, M. Kubicki, S. K. Hadjikakou, Polyhedron **67** (2014) 89-103.

[15] N. Arora, D. Goutam, I. Wachs, A. Hirt, J. Catal. **159** (1996) 1-13.

[16] P. Majewski, J. Mater. Res. **15** (2000) 854-870.

[17] J. Fu, J. Mater. Sci. Lett. **16** (1997) 1433-1436.

[18] W. E. Mahmoud, A. A. Al-Ghamdi, Polym. Adv. Technol. **22** (2011) 877-881.

[19] K. L. Chopra, S. R. Das, Plenum Press, New York 1983.

[20] G. M. Sheldrick, Acta Crystallogr., Sect. A: Found. Crystallogr. **64** (2008) 112-122.

[21] M. J. Frisch, G. W. Trucks, H. B. Schlegel, G. E. Scuseria, M. A. Robb, J. R. Cheeseman, G. Scalmani, V. Barone, B. Mennucci, G. A. Petersson, H. Nakatsuji, M. Caricato, X. Li, H. P. Hratchian, A. F. Izmaylov, J. Bloino, G. Zheng, J. L. Sonnenberg, M. Hada, M. Ehara, K. Toyota, R. Fukuda, J. Hasegawa, M. Ishida, T.

Nakajima, Y. Honda, O. Kitao, H. Nakai, T. Vreven, J. A. Montgomery Jr., J. E. Peralta, F. Ogliaro, M. Bearpark, J. J. Heyd, E. Brothers, K. N. Kudin, V. N. Staroverov, R. Kobayashi, J. Normand, K. Raghavachari, A. Rendell, J. C. Burant, S. S. Iyengar, J. Tomasi, M. Cossi, N. Rega, J. M. Millam, M. Klene, J. E. Knox, J. B. Cross, V. Bakken, C. Adamo, J. Jaramillo, R. Gomperts, R. E. Stratmann, O. Yazyev, A. J. Austin, R. Cammi, C. Pomelli, J. W. Ochterski, R. L. Martin, K. Morokuma, V. G. Zakrzewski, G. A. Voth, P. Salvador, J. J. Dannenberg, S. Dapprich, A. D. Daniels, O. Farkas, J. B. Foresman, J. V. Ortiz, J. Cioslowski, D. J. Fox, Gaussian 09, Revision D.01, Gaussian Inc. Wallingford CT, 2009.

[22] P. Jamunarani, S. Thirumaran, Eur. J. Med. Chem. **62** (2013) 139-147.

[23] N. Awang, I. Baba, B. M. Yamin, M .S. Othmam, N. F. Kamaludin, Am. J. Applied. Sci. **8** (2011) 310-317.

[24] (a) T. Mosmann, J. Immunol. Methods. 1983, **65**, 55-63.
(b) N. Awang, N. S. A. Mohd Yousof, N. F. Rajab, N. F. Kamaludin, J. App. Pharm. Sci. **5** (2015) 007-011.

[25] H. O. Hassani, S. Rakass, F. T. Al Wadaani, J. Khalaf. Al-ghamdi, A. Omer, M. M. Abboudi, J. Taibah. Univ. Sci. **9** (2015) 508-512.

[26] F. Bonati, R. Ugo, J. Organomet. Chem. **10** (1967) 257-268.

[27] L. Ronconi, L. Giovagnini, C. Marzano, F. Bettio, R. Graziani, G. Pilloni, D. Fregona, Inorg. Chem. **44** (2005) 1867-1881.

[28] R. Baggio, A. Frigerio, E. B. Halac, D. Vega and M. Perec, J. Chem. Soc, Dalton Trans. 1992, 549-554

[29] H. L. M. Van Gaal, J. W. Diesveld, F. W. Pijipers, J. G. M. Van der Linden, Inorg.Chem. **18** (1979) 3251-3260.

[30] E. Sathiyaraj, T. Srinivasan, S. Thirumaran, D. Velmurugan, J. Mol. Struct. **1102** (2015) 203-209.

[31] M. K. Bharty, R. K. Dani , P. Nath , A. Bharti , N. K. Singh, Om Prakash , R. K. Singh, R. J. Butcher, Polyhedron **98** (2015) 84-95.

[32] R. K. Singh, S. K. Verma, P. D. Sharma, Int. J. Chem. Tech. Res. **3** (2011) 1571-1579.

[33] G. H. Hwang , W. K. Han, S. J. Kim, S. J. Hong, J. S. Park, H. J. Park, S. G. Kang, J. Ceram. Process. Res. **10** (2009) 190-194.

[34] M. J. Jabeen Fatima, C. V. Niveditha, S. Sindhu, RSC Adv. **5** (2015) 78299-78305.

[35] S. K. Sengupta, S. kumar, Thermochim. Acta. **72** (1984) 349-361.

[36] L. Leontie, M. Caraman, M. Delibas, G. I. Rusu, Mater. Res. Bull. **36** (2001) 1629-1637.

Scheme and Figure captions

Scheme 1. Preparation of the complexes **1-3**

Figure 1. ORTEP diagram of complex **3** at 40% probability

Figure 2. The dimeric structure of **3** predicted by Bi···S and C-H···O interactions

Figure 3. Intermolecular C–H···π (chelate) and C–H···π interactions in complex **3**

Figure 4. Frontier molecular orbital diagram of complex **3**

Figure 5. **(a)** Electrostatic potential surface and (**b**) Contour map of electrostatic Potential of complex **3**

Figure 6. Antimicrobial activity of complexes **1-3** against tested organisms

Figure 7. Percentage of cell viability at different concentrations of complexes **1-3**

Figure 8. X-ray di□raction pattern of the as-synthesized bismuth oxide NPs

Figure 9. HR-TEM images of bismuth sulfide NPs, scale bars (a) 200 nm, (b) 100 nm, (c) 10 nm and (d) Selected area electron diffraction (SAED) pattern of the as-synthesized bismuth oxide NPs

Figure 10. (**a**) UV-Vis spectra and (**b**) Photoluminescence spectra of the as-synthesized bismuth oxide nanoparticles

Figure 11. Time-dependent UV-Vis absorption spectra for decolorization of rhodamine- B using as-prepared Bi_2O_3

Table 1 Crystal data, data collection and refinement parameters for complex **3**

Empirical formula	$C_{39}\ H_{36}\ Bi\ N_3\ O_3\ S_6$
FW	996.05
Crystal dimensions (mm)	$0.3 \times 0.282 \times 0.25$
Crystal system	monoclinic
Space group	$P\ 2_1/n$
a/Å	10.5715(3)
b/Å	11.7179(3)
c/Å	32.0535(9)
α/°	90.00
β/°	96.744(3)
γ/°	90.00
V/Å^3	3943.18(19)
Z	4
Dc/g cm^{-3}	1.678
μ/cm^{-1}	4.831
F(000)	1976
λ/Å	MoK_α (0.71073)
θ Range/°	4.2460 – 31.1350
Index ranges	$-16 \le h \le 15, -16 \le k \le 14,$ $-43 \le l \le 48$
Reflections collected	13195
Observed reflections [$I > 2\sigma(I)$]	9769
Weighting scheme	Calc.$W=1/[\sigma^2(F_o^2)+(0.0493P)^2 + 6.6827P]$ where $P = (F_o^2+2F_c^2)/3$
Number of parameters refined	469
R[$F^2 > 2\sigma(F^2)$], wR(F^2)	0.0777, 0.1188
GOOF	0.961

Table. 2 Selected bond distances (Å) and bond angles (°) for the complex **3.**

3							
S1-Bi1	2.5876(12)	C20-N2	1.469(6)	S2-Bi1-S1	65.65(3)	C1-N1-C2	122.2(4)
S2-Bi1	2.8747(12)	C15-N2	1.467(6)	S6-Bi1-S1	85.70(4)	S4-C14-S3	119.9(3)
S3-Bi1	2.8056(12)	C27-S6	1.722(5)	S5-Bi1-S6	63.02(3)	N2-C14-S3	120.0(3)
S4-Bi1	2.9055(13)	C27-S5	1.727(5)	S5-Bi1-S4	158.24(3)	N2-C14-S4	120.2(3)
S5-Bi1	2.8886(12)	C27-N3	1.324(6)	S3-Bi1-S4	62.47(3)	C14-N2-C15	121.7(4)
S6-Bi1	2.7711(13)	C33-N3	1.478(6)	S3-Bi1-S2	136.46(4)	C14-N2-C20	122.4(4)
C1-S1	1.748(5)	C28-N3	1.467(6)	C1-S1-Bi1	91.53(17)	C15-N2-C20	115.4(4)
C1-N1	1.327(6)			C1-S2-Bi1	83.30(17)	S6-C27-S5	118.2(3)
C1-S2	1.692(5)			N1-C1-S1	117.9(3)	N3-C27-S5	121.4(3)
C7-N1	1.471(6)			N1-C1-S2	122.6(3)	N3-C27-S6	120.4(3)
C2-N1	1.489(6)			S1-C1-S2	119.4(3)	C33-N3-C27	123.1(4)
C14-S3	1.719(5)			C2-N1-C7	113.7(4)	C28-N3-C27	122.6(4)
C14-S4	1.705(5)			C7-N1-C1	124.2(4)	C28-N3-C33	113.9(4)
C14-N2	1.357(6)						

Table 3 Selected bond parameters (theoretical and experimental) for **3**

Bond distances (Å)	XRD	DFT/ LAN2DZ	Bond angle(°)	XRD	DFT/ LAN2DZ
Bi1-S1	2.5876(12)	2.9845	S2-Bi1-S1	65.65(3)	64.03
Bi1-S2	2.8747(12)	2.8364	S3-Bi1-S1	88.59(4)	81.53
Bi1-S3	2.8056(12)	3.0467	S4-Bi1-S3	62.47(3)	64.96
Bi1-S4	2.9055(13)	2.6737	S6-Bi1-S5	63.02(3)	63.59
Bi1-S5	2.8886(12)	2.9921	N1-C1-S1	117.9(3)	121.46
Bi1-S6	2.7711(13)	2.8536	N1-C1-S2	122.6(3)	119.68
N1-C1	1.327(6)	1.3525	S1-C1-S2	119.4(3)	118.85
S1-C1	1.748(5)	1.7803	N2-C14-S3	120.0(3)	123.31
S2-C1	1.692(5)	1.8071	N2-C14-S4	120.2(3)	117.93
N2-C14	1.357(6)	1.3550	S3-C14-S4	119.9(3)	118.75
S3-C14	1.719(5)	1.7592	N3-C27-S5	121.4(3)	121.38
S4-C14	1.705(5)	1.8291	N3-C27-S6	120.4(3)	120.01
N3-C27	1.324(6)	1.3576	S5-C27-S6	118.2(3)	118.60
S5-C27	1.727(5)	1.7833			
S6-C27	1.722(5)	1.8011			

Graphical abstract (synopsis)

Three new Bi(III) dithiocarbamates have been prepared and characterized. X-ray structure of **3** shows that Bi is in distorted pentagonal pyramidal environment. Cytotoxic activity against KB(cell) **1-3** with IC_{50} = 44, 85 and 40 µg/ml, respectively. Thermal decomposition of 3 yielded α-Bi_2O_3 nanobars. Optical, structural and photocatalytic properties of α-Bi_2O_3 were evaluated.

Graphical Abstract

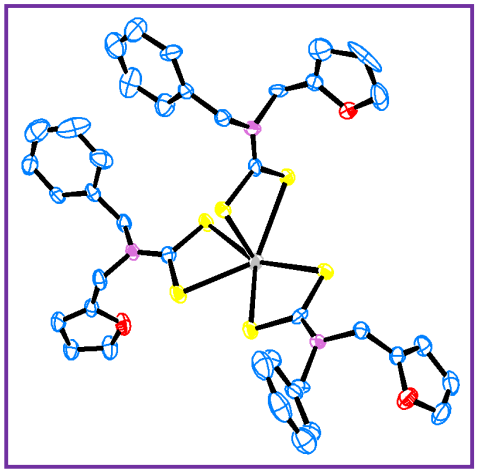

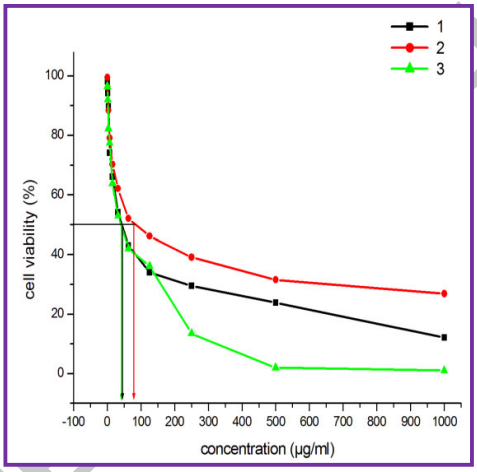

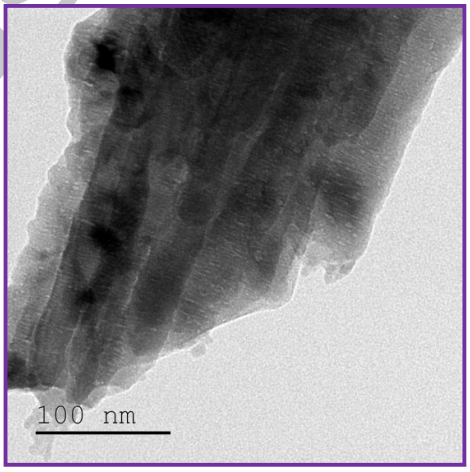

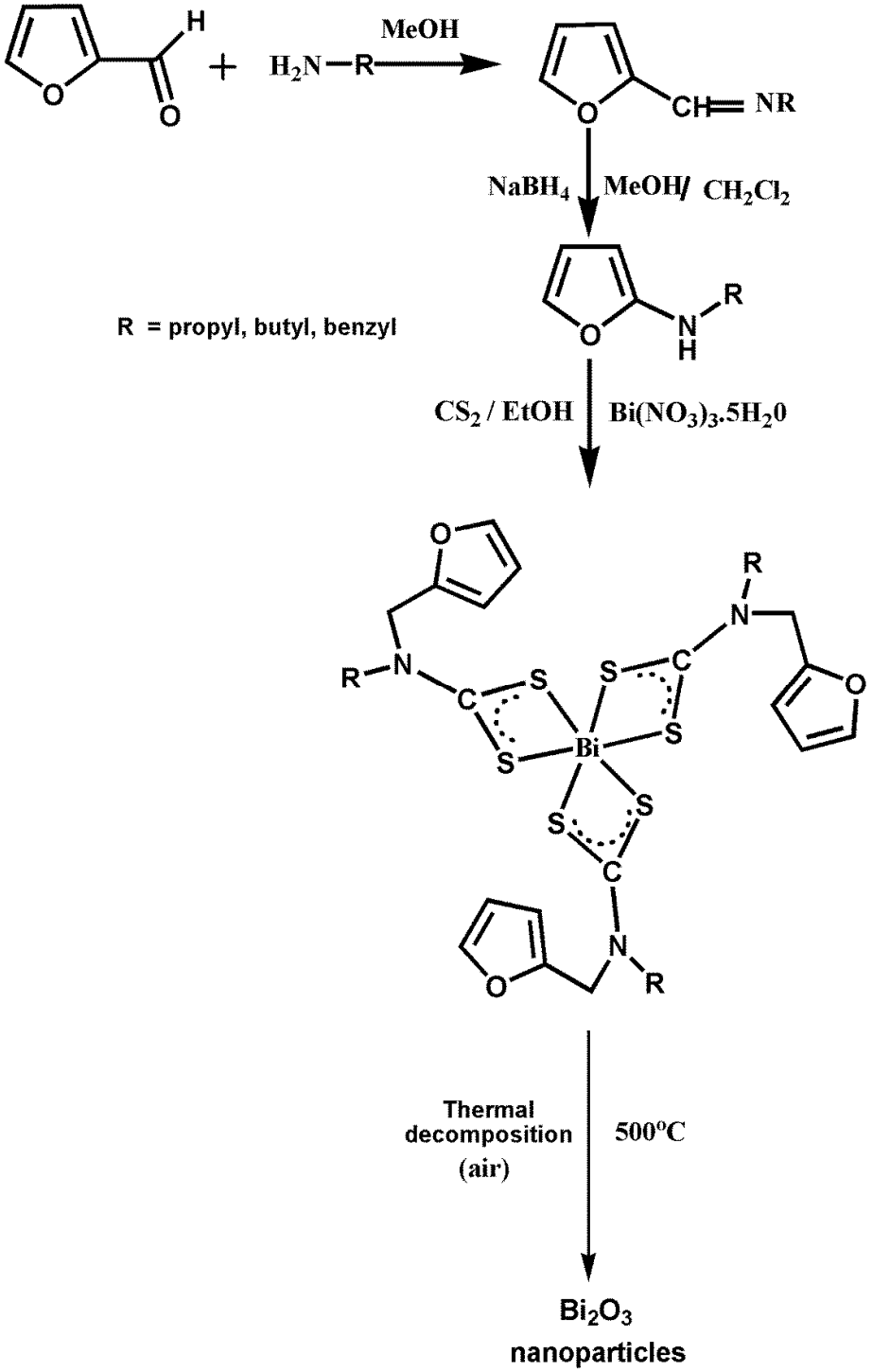

Scheme 1.

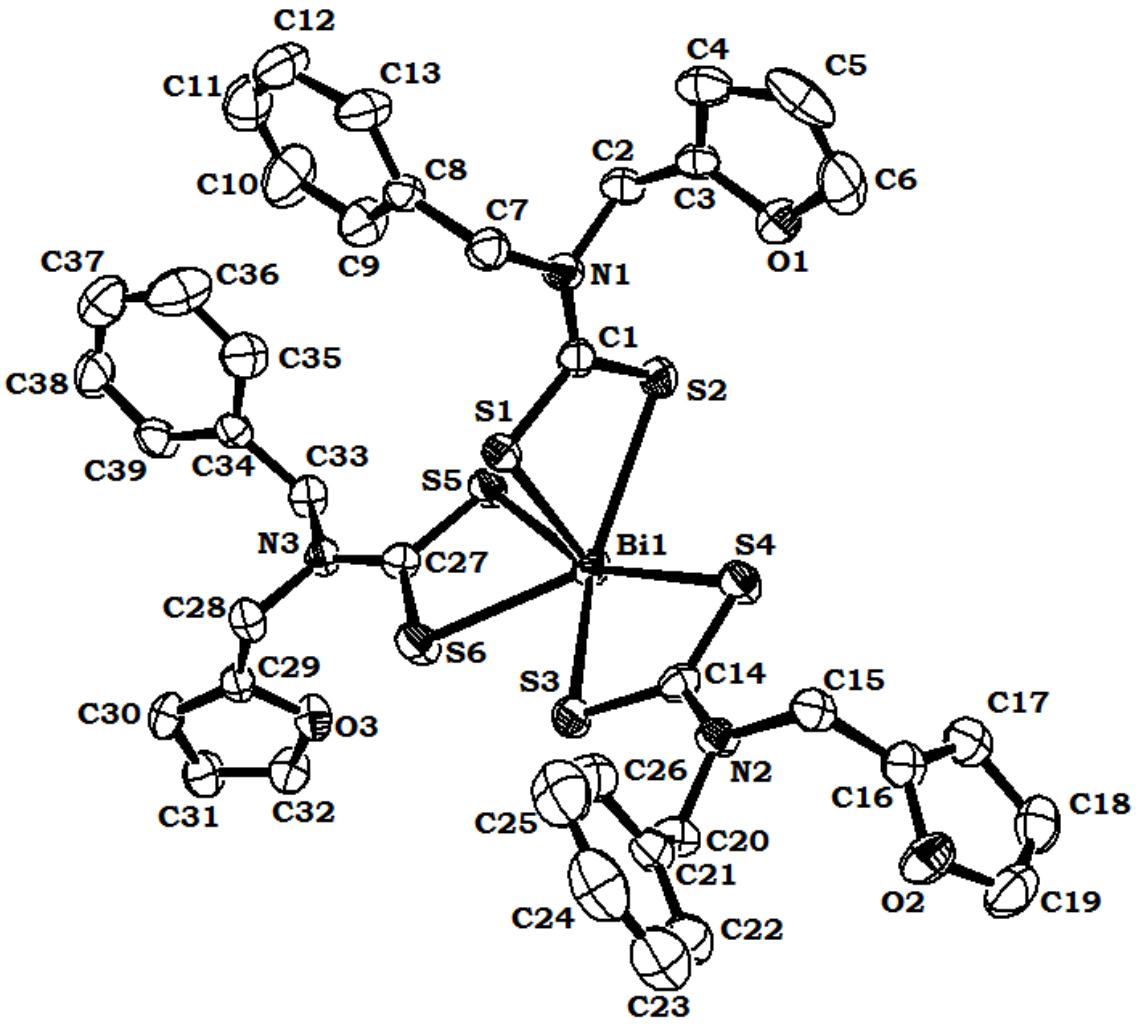

Figure 1.

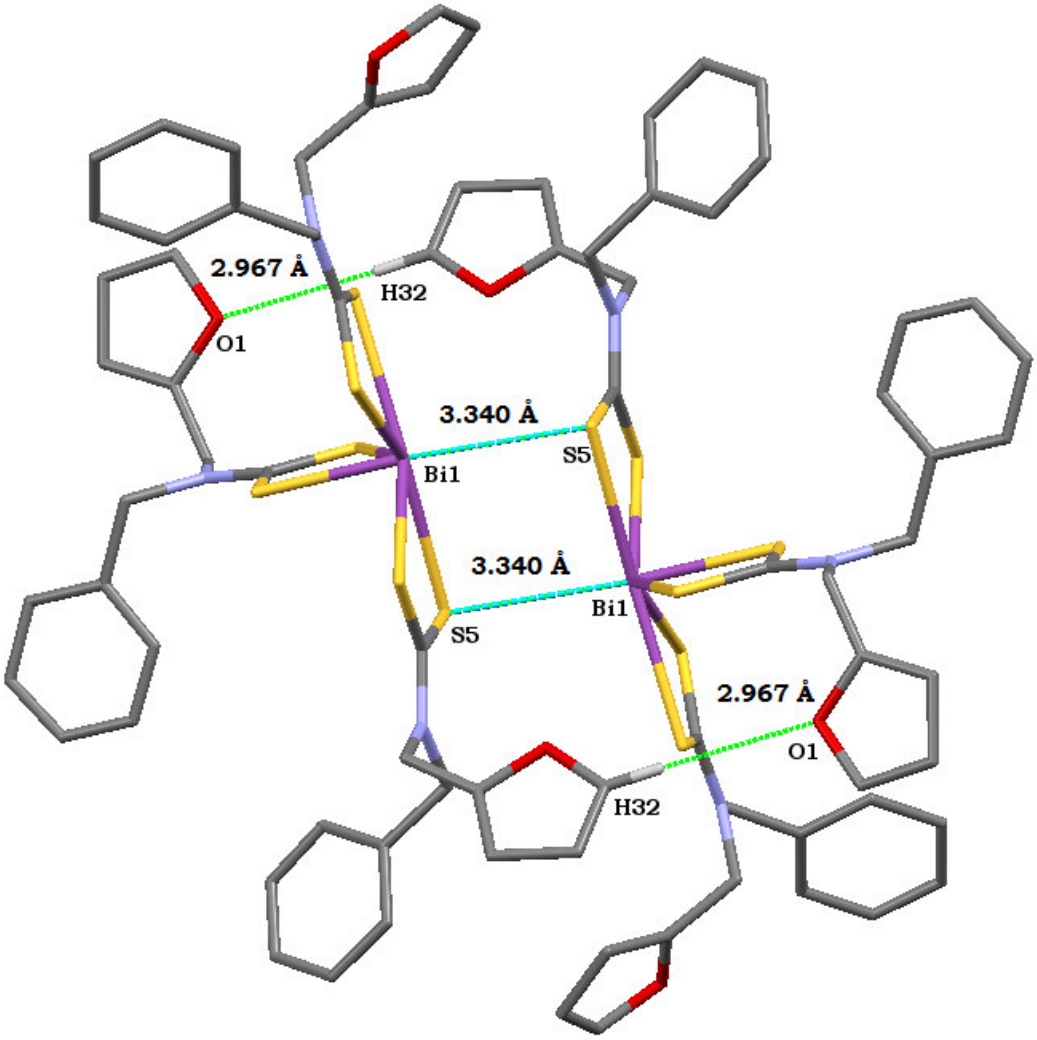

Figure 2.

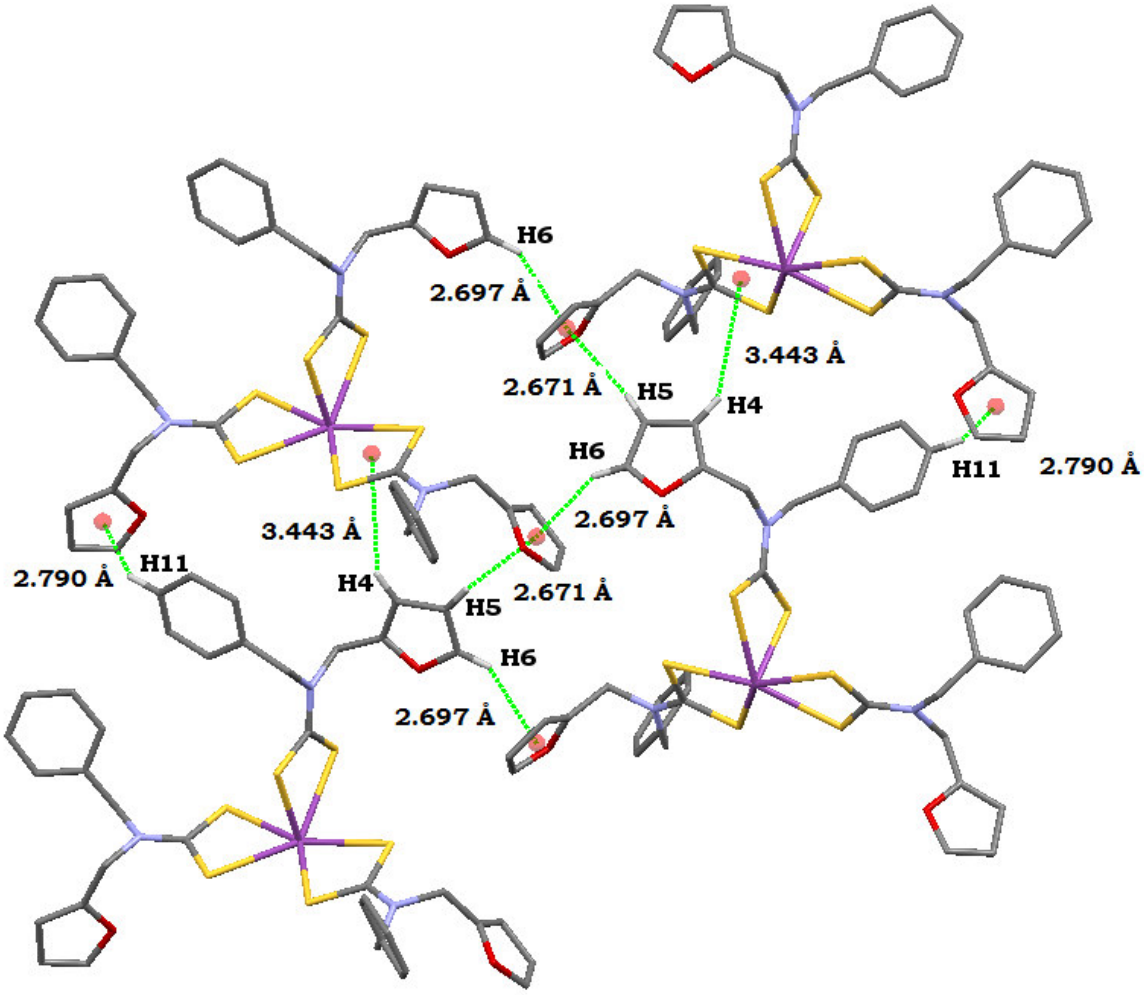

Figure 3.

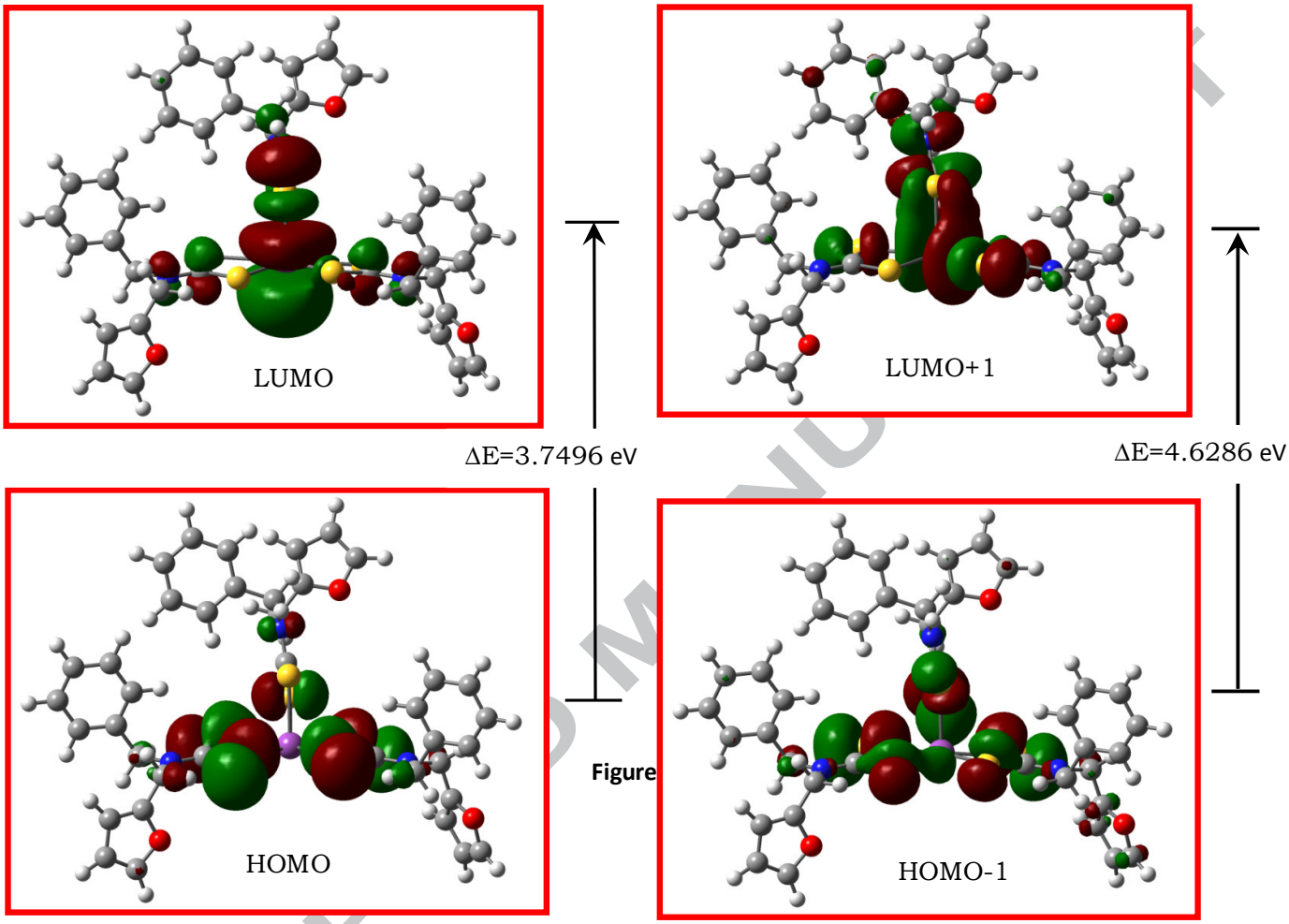

Figure

Figure 4.

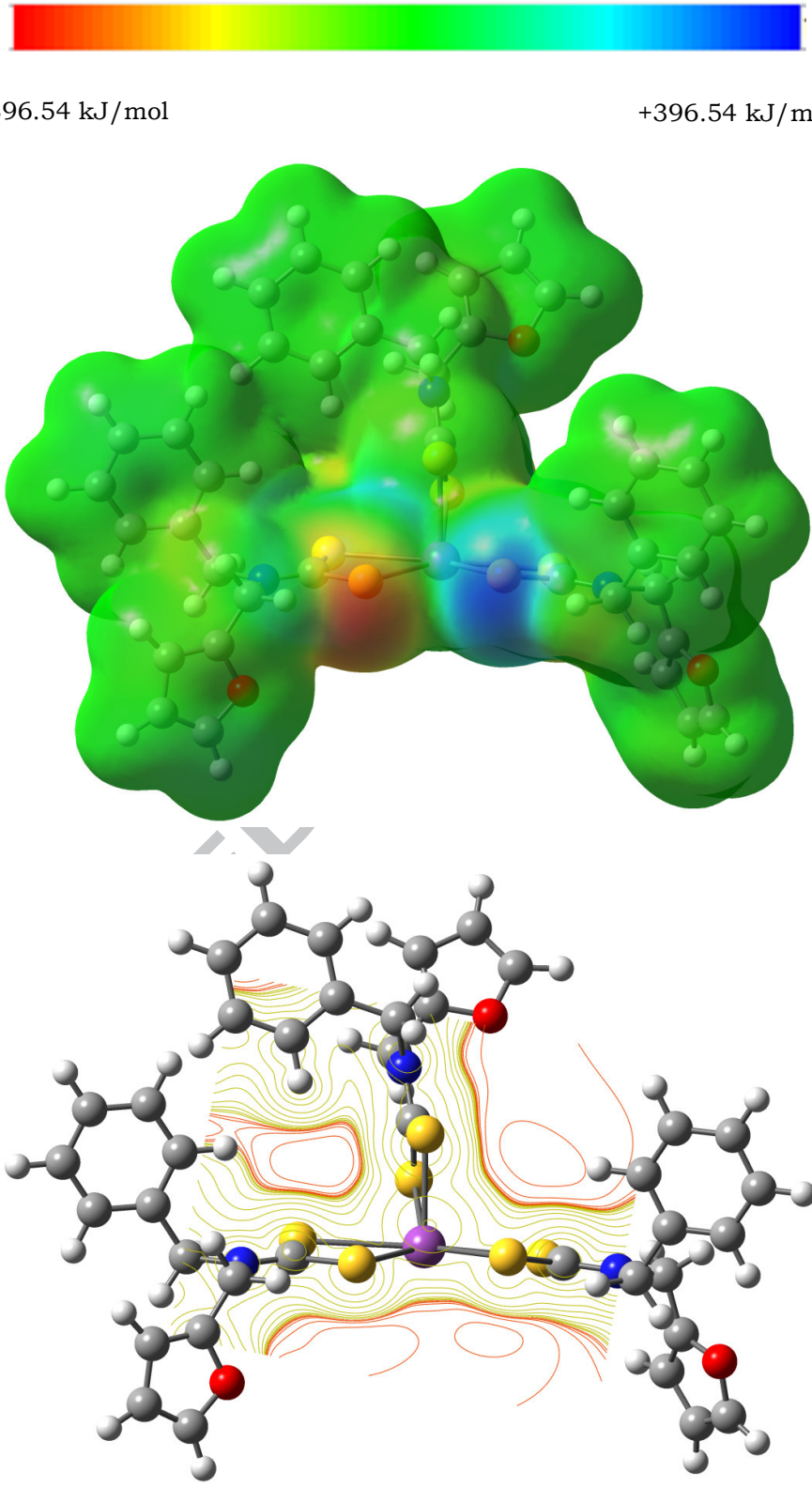

Figure 5.

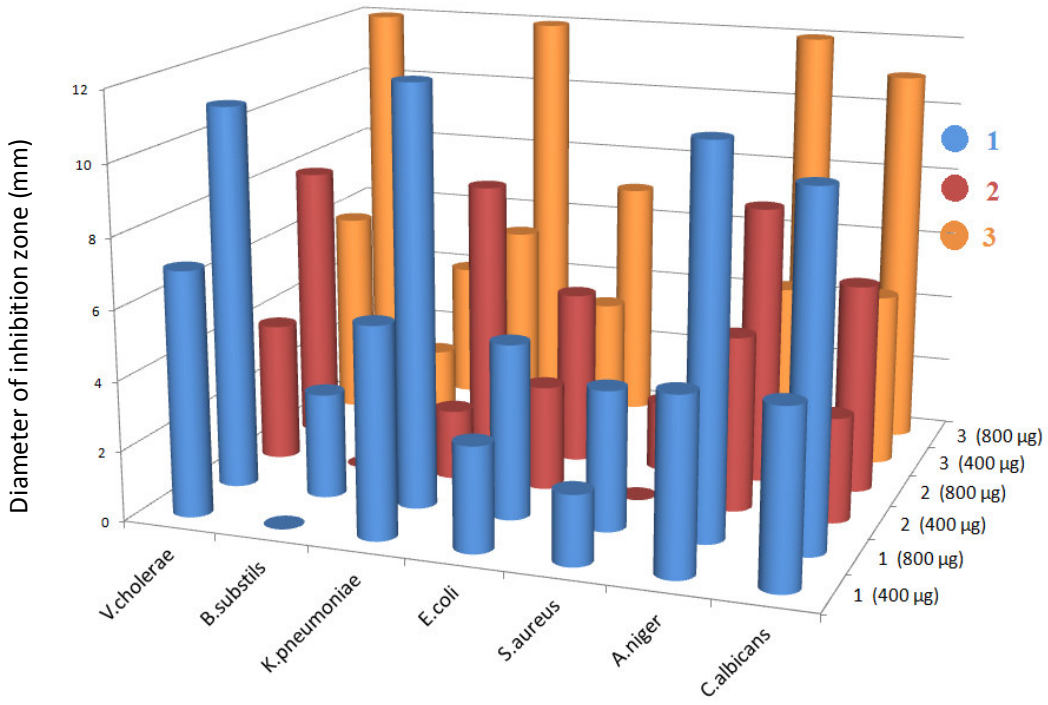

Figure 6.

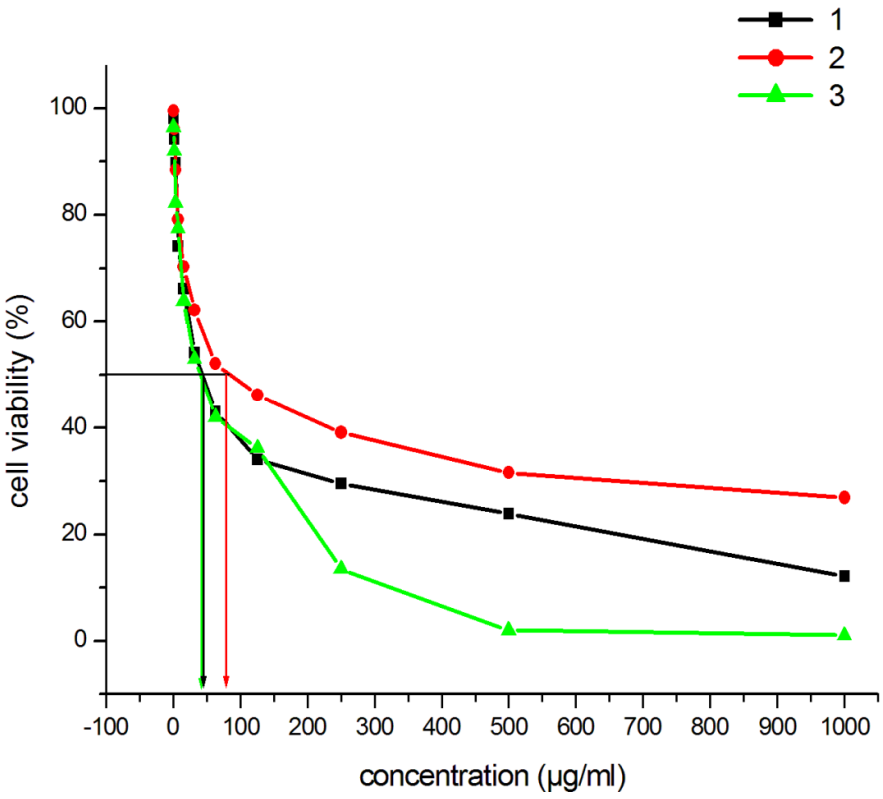

Figure 7.

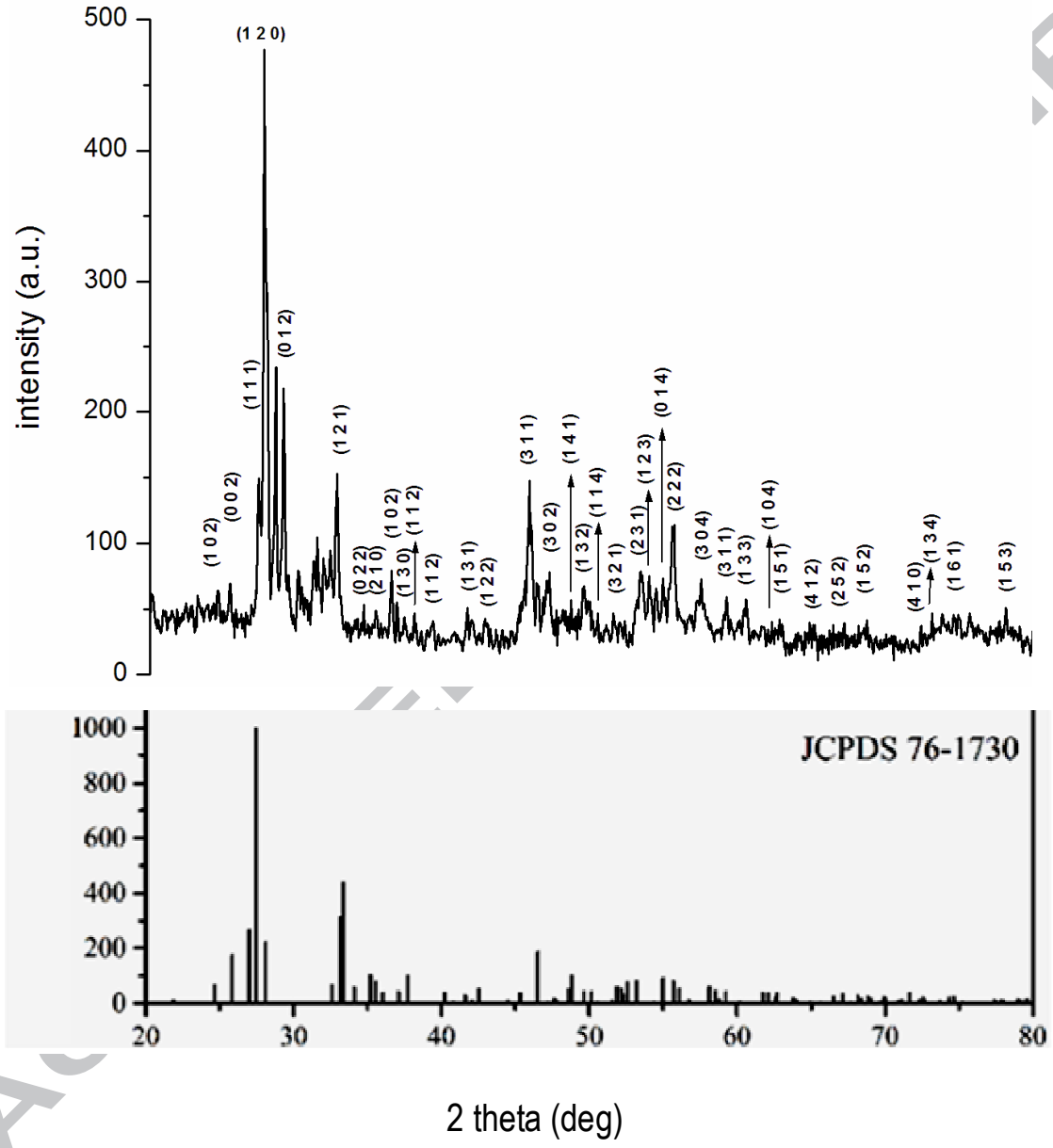

Figure 8.

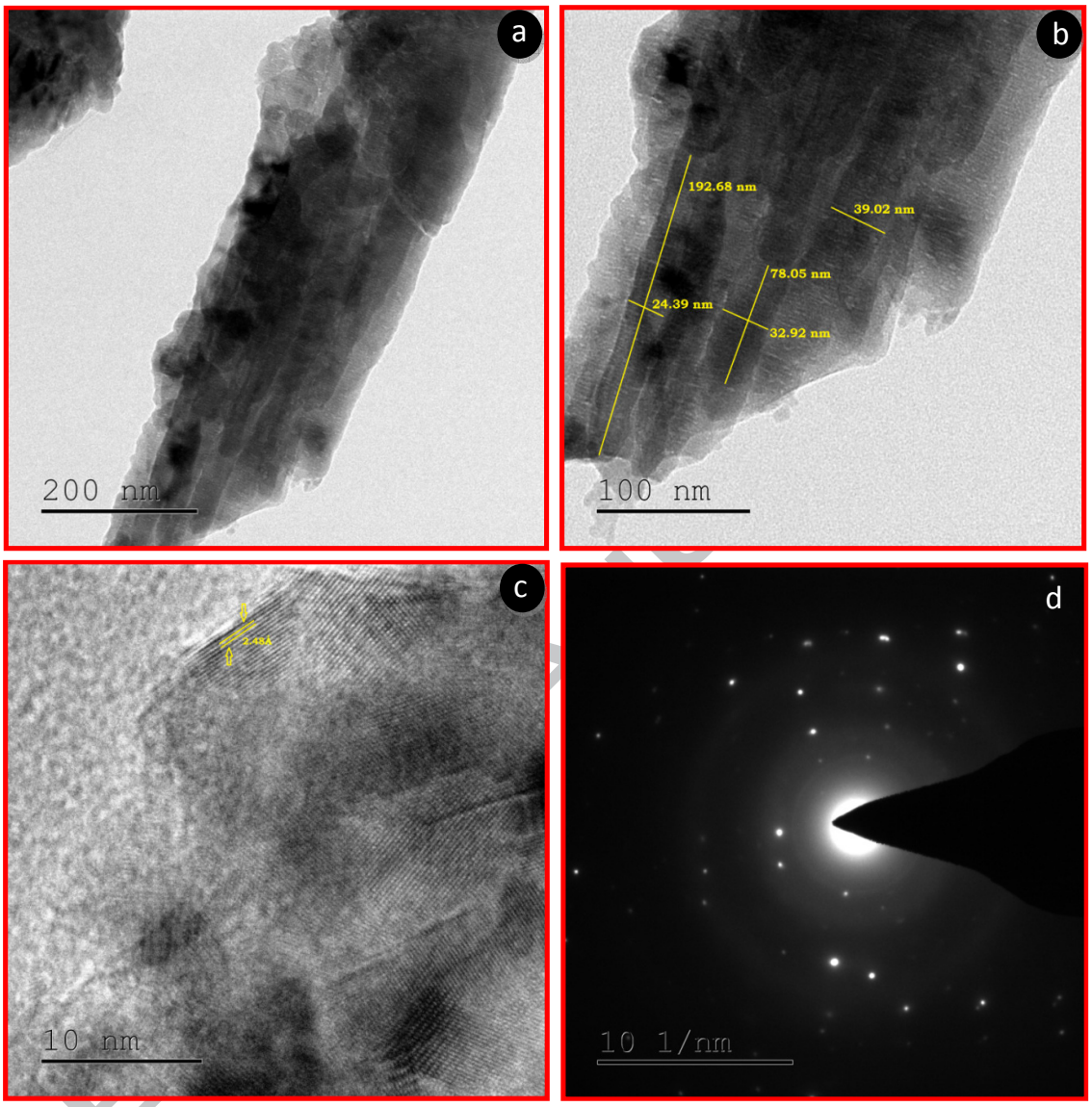

Figure 9.

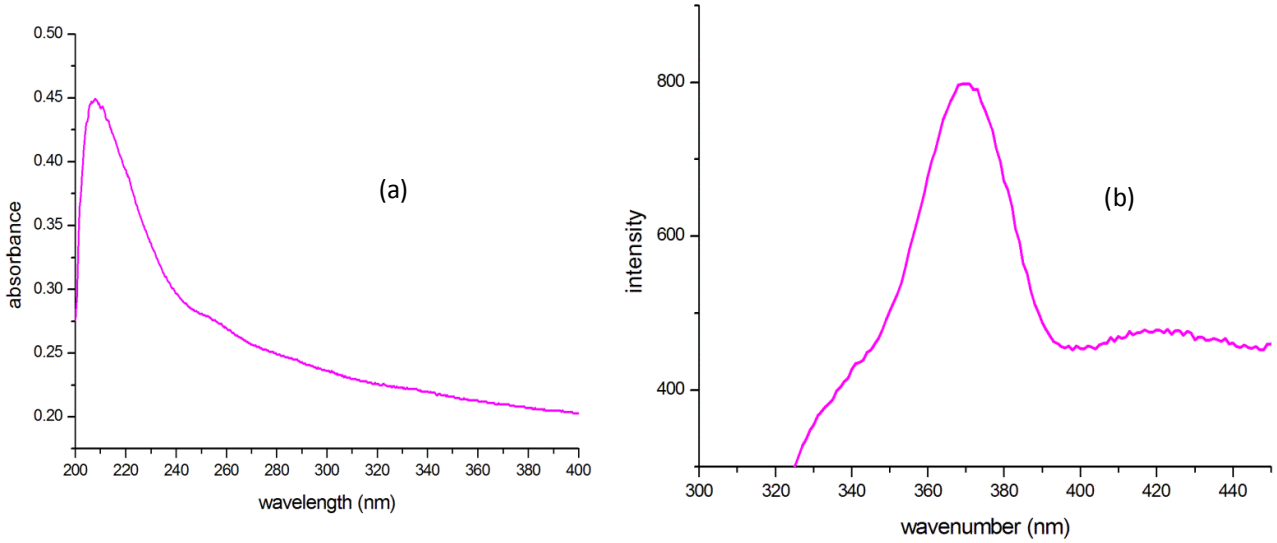

Figure 10.

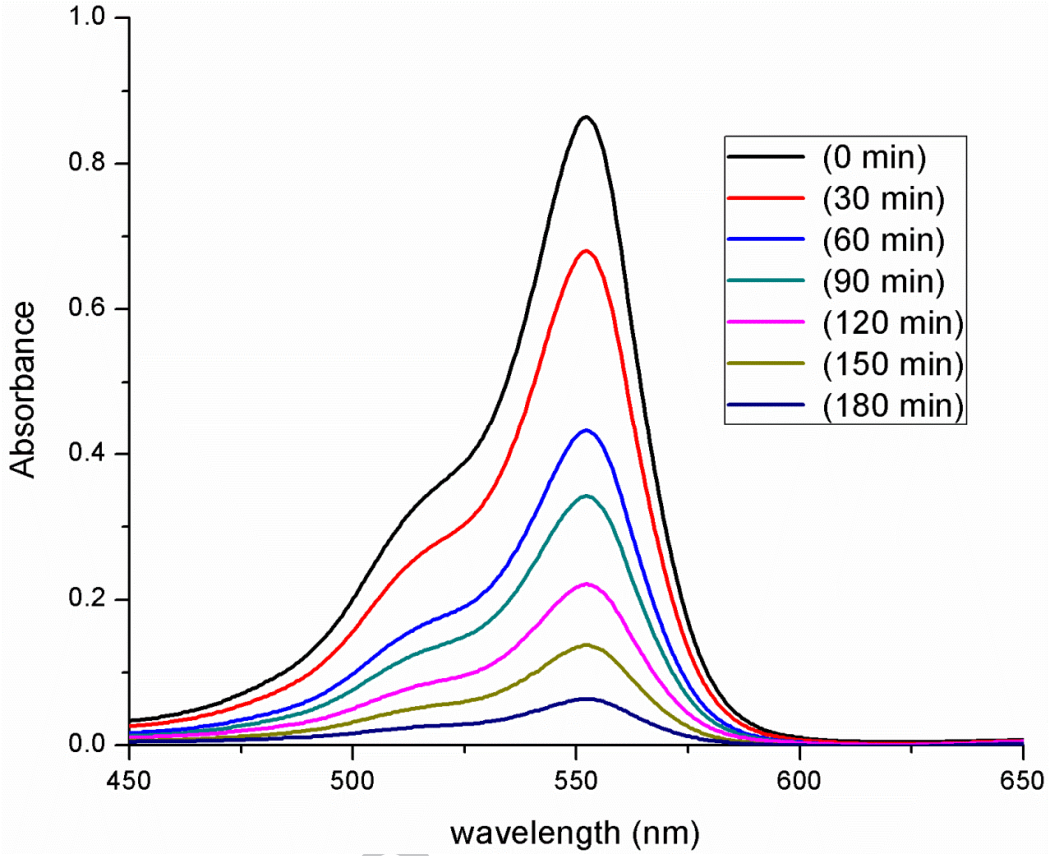

Figure 11.